
HANDLING THE NON-SMOOTH CHALLENGE IN TENSOR SVD: A MULTI-OBJECTIVE TENSOR RECOVERY FRAMEWORK

Jingjing Zheng

Department of Mathematics
The University of British Columbia
British Columbia, Canada
jjzheng@math.ubc.ca

Wanglong Lu

Department of Computer Science
Memorial University of Newfoundland
Newfoundland and Labrador, Canada
wanglongl@mun.ca

Wenzhe Wang

College of Computer Science and Artificial Intelligence
Wenzhou University
Zhejiang, China
wangwenzhe@qdpcc.edu.cn

Yankai Cao*

Department of Chemical and Biological Engineering
University of British Columbia
British Columbia, Canada
yankai.cao@ubc.ca

Xiaoqin Zhang

College of Computer Science and Artificial Intelligence
Wenzhou University
Zhejiang, China
zhangxiaoqinnan@gmail.com

Xianta Jiang

Department of Computer Science
Memorial University of Newfoundland
Newfoundland and Labrador, Canada
xiantaj@mun.ca

ABSTRACT

Recently, numerous tensor singular value decomposition (t-SVD)-based tensor recovery methods have shown promise in processing visual data, such as color images and videos. However, these methods often suffer from severe performance degradation when confronted with tensor data exhibiting non-smooth changes. It has been commonly observed in real-world scenarios but ignored by the traditional t-SVD-based methods. In this work, we introduce a novel tensor recovery model with a learnable tensor nuclear norm to address such challenge. We develop a new optimization algorithm named the Alternating Proximal Multiplier Method (APMM) to iteratively solve the proposed tensor completion model. Theoretical analysis demonstrates the convergence of the proposed APMM to the Karush–Kuhn–Tucker (KKT) point of the optimization problem. In addition, we propose a multi-objective tensor recovery framework based on APMM to efficiently explore the correlations of tensor data across its various dimensions, providing a new perspective on extending the t-SVD-based method to higher-order tensor cases. Numerical experiments demonstrated the effectiveness of the proposed method in tensor completion.

1 Introduction

In recent years, lots of tensor methods have been proposed to better analyze the low-rankness in massive high-dimensional tensor data, including color images, hyperspectral images, and videos [1, 2, 3, 4, 5, 6], as the traditional matrix methods [7, 8, 9, 10, 11, 12] fail on handling the tensor data. Depending on different adopted low-rank prior, these tensor methods can be categorized as: (1) CP (Canonical Polyadic) Decomposition-based methods [13, 14, 15], (2) Tucker Decomposition-based methods [16, 17, 18], and (3) t-SVD-based methods [4, 5, 19, 20].

Recently, the t-SVD-based methods have gained increasing attention and achieved great success in the applications of visual data processing, such as data denoising [2], image and video inpainting [3, 4, 5], and background modeling and

*Corresponding Author

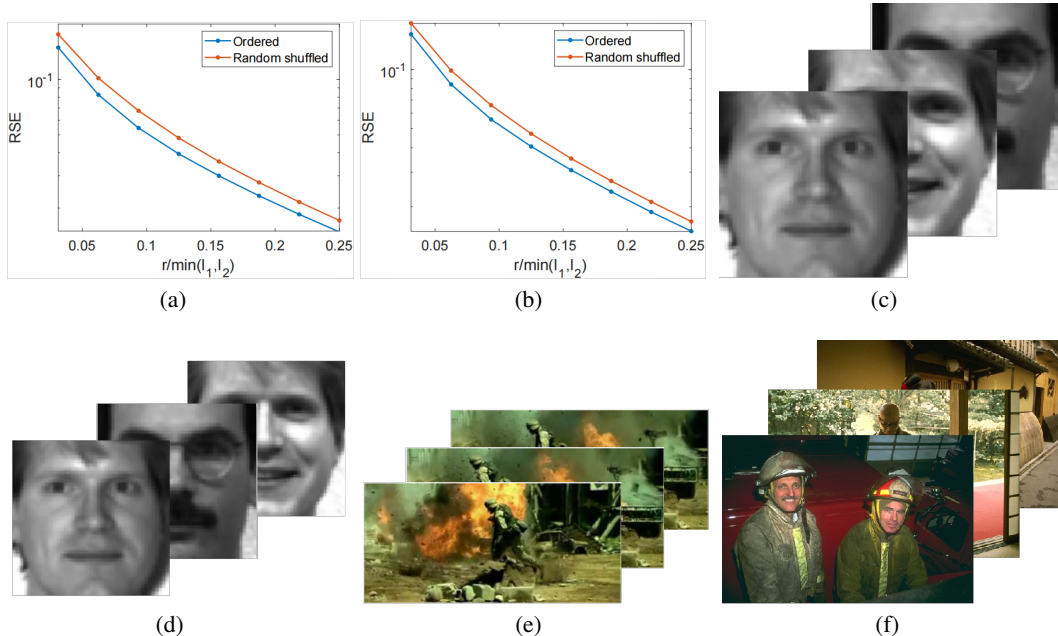


Figure 1: Illustration to challenges of t-SVD-based methods in real world scenarios: (a) comparison of DFT-based t-SVD on yale dataset in ordered and random shuffled; (b) comparison of DCT-based t-SVD on yale dataset in ordered and random shuffled; (c) ordered images; (d) disordered images for classification task; (e) video with rapidly changing frames; (f) image sequence with different scenes.

initialization [2, 21]. In these t-SVD-based methods, a fixed invertible transform, such as Discrete Fourier Transform (DFT) [5] and Discrete Cosine Transform (DCT) [4], is applied to a tensor data along its certain dimension. The low-rankness prior of each frontal slice of the transformed tensor has been used to explore global low-rankness of tensor data. However, the approach of performing invertible transform and analyzing the low rankness along a specific dimension of tensor data poses the following challenges, namely: (i) non-smooth challenge, and (ii) the lack of an effective way to generalize t-SVD-based methods directly to higher-order tensor cases.

Regarding the non-smooth challenge, Fig. 1 illustrates two different real-world scenarios: disordered images sequence (Fig. 1 (a)-(d)) and tensor data with non-smooth changes (Fig. 1 (e)-(f)). These commonly encountered scenarios pose a significant challenge for t-SVD-based tensor analysis methods. Taken an example illustrated in Fig. 1 (a)-(d), the disordered images sequence often affect the tensor recovery performance significantly. This phenomenon is referred as to tensor slices permutation variability (SPV) [22], *i.e.*, interchanging the frontal slice of the tensor will affect the t-SVD results. Since the sequence of samples is often disordered prior to classification, this phenomenon is frequently observed within classification tasks. Although Zheng *et al.* have proposed an effective solution for handling such issue by solving a Minimum Hamiltonian circle problem for the case of DFT [22], a general solution is still lacking. In addition, the recovery performance of the t-SVD-based methods is also susceptible to non-smooth of the tensor data itself [23]. These data include videos with rapidly changing content between frames and tensor data obtained by concatenating images with different scenes as illustrated in Fig. 1 (e) and (f), respectively. These non-smooth challenges arise because a fixed invertible transform, such as DFT or DCT, is applied to the tensor along certain dimensions, making the t-SVD sensitive to disorder and non-smooth changes in tensor slices.

To address the mentioned second challenge, a common solution for handling high-order tensors is to utilize tensor unfolding operators [19, 20]. For example, in [19], the Weighted Sum of Tensor Nuclear Norm of all mode- (k_1, k_2) unfolding tensors (WSTNN) has been proposed to investigate correlations along different modes of higher order tensors. However, the consideration of weighted summation in WSTNN results in a challenging setting requiring $h(h-1)/2$ weight parameters.

1.1 Our Contributions

This study aims to address the above two challenges, and our contributions are as follows.

Table 1: Notations

| Notations | Descriptions | Notations | Descriptions |
|---|---|---|--|
| a, b, c, \dots | scalars | $\mathbf{a}, \mathbf{b}, \mathbf{c}, \dots$ | vectors |
| $\mathbf{A}, \mathbf{B}, \mathbf{C}, \dots$ | matrices | $\mathcal{A}, \mathcal{B}, \mathcal{C}, \dots$ | tensors |
| $\mathbb{A}, \mathbb{B}, \mathbb{C}, \dots$ | sets | $\mathcal{A}, \mathcal{B}, \mathcal{C}, \dots$ | operators |
| $[1 : n]$ | $\{1, 2, \dots, h\}$ | \mathbf{F}_{I_n} | Discrete Fourier Matrix (DFM) with size of $I_n \times I_n$ |
| \mathbf{A}^T | transpose of \mathbf{A} | $[\mathcal{A}]_{i_1, i_2, \dots, i_h}$ | (i_1, i_2, \dots, i_h) -th element of \mathcal{A} |
| \mathcal{I} | identity tensor | $\mathbf{0}$ | null tensor |
| $\mathcal{A}^{T_{k_1, \dots, k_h}}$ | rotation of $\mathcal{A} \in \mathbb{R}^{I_1 \times \dots \times I_h}$ such that $\mathcal{A}^{T_{k_1, \dots, k_h}} \in \mathbb{R}^{I_{k_1} \times \dots \times I_{k_h}}$ | $\mathcal{A}_{(k)}$ (or $[\mathcal{A}]_{(n)}$) | Mode- n Unfolding of \mathcal{A} |
| $[\mathcal{A}^{T_{k_1, \dots, k_h}}]_{::, i_{k_3}, \dots, i_{k_h}}$ | slice along the (k_1, k_2) -th mode | \times_n | Mode- n product |
| $\ \mathcal{A}\ _0$ | the number of non-zero elements of \mathcal{A} | $\ \mathcal{A}\ _1$ | $\ \mathcal{A}\ _1 = \sum_{i_1, i_2, \dots, i_h} [\mathcal{A}]_{i_1, i_2, \dots, i_h} $ |
| \mathbb{A}^c | complementary set of \mathbb{A} | $ \mathbb{A} $ | number of elements of \mathbb{A} |

- We proposed a new tensor recovery model with a learnable tensor nuclear norm by introducing a set of unitary matrices to effectively address SPV and non-smoothness issues in the traditional t-SVD-based methods, thereby allowing our model to harness the inherent data characteristics.
- We presented a novel optimization algorithm named the Alternating Proximal Multiplier Method (APMM) to solve the proposed tensor recovery model effectively, along with a corresponding convergence analysis in theory.
- We are the first in the literature to propose a multi-objective tensor recovery with learned tensor nuclear norms for effectively exploring the low-rankness of tensor data across its various dimensions, without the need for introducing numerous tensor variables and weights as in traditional weighted sum-based methods [19, ?]. The experimental results demonstrates the superior performance in tensor completion than other methods. For instance, the proposed framework has achieved a 3.5 dB improvement in color video inpainting!

2 Multi-Objective Tensor Recovery with Learnable Tensor Nuclear Norms

Before introducing our problem and the proposed methods, we summarize notations in Table 1 that will be used later.

2.1 Tensor Completion Problem

Considering tensor data $\mathcal{M} \in \mathbb{R}^{I_1 \times I_2 \times \dots \times I_h}$ may with missing elements, [4, 20] propose the following t-SVD-based tensor completion model:

$$\min_{\mathcal{X}} \text{rank}_{[k_1, k_2]}(\mathcal{X}) \quad s.t. \quad \Psi_{\mathbb{I}}(\mathcal{M}) = \Psi_{\mathbb{I}}(\mathcal{X}), \quad (1)$$

where $\Psi_{\mathbb{I}}$ is a linear project operator on the support set \mathbb{I} such that

$$[\Psi_{\mathbb{I}}(\mathcal{M})]_{i_1, i_2, \dots, i_h} = \begin{cases} [\mathcal{M}]_{i_1, i_2, \dots, i_h}, & \text{if } (i_1, i_2, \dots, i_h) \in \mathbb{I}; \\ 0, & \text{if } (i_1, i_2, \dots, i_h) \notin \mathbb{I}, \end{cases}$$

and $i_k \in [1 : I_k]$ for $k = 1, 2, \dots, h$. The tensor rank function in (1) operates on the assumption that an h -order tensor data $\mathcal{M} \in \mathbb{R}^{I_1 \times I_2 \times \dots \times I_h}$ in the real world can be decomposed as

$$\mathcal{M} = \mathcal{Z} \times_{k_3} \hat{\mathbf{U}}_{k_3}^T \cdots \times_{k_h} \hat{\mathbf{U}}_{k_h}^T, \quad (2)$$

where $\{k_3, k_4, \dots, k_h\} \subset [1 : h]$, $\{\hat{\mathbf{U}}_{k_n}\}_{n=3}^h$ are a set of given invertible transforms, and

$$\text{rank}_{[k_1, k_2]}(\mathcal{M}) = \max_{i_{k_n} \in [1 : I_{k_n}] \text{ for } n=3, 4, \dots, h} \text{rank} \left([\mathcal{Z}^{T_{k_1, \dots, k_h}}]_{::, i_{k_3}, \dots, i_{k_h}} \right) \ll \min(I_{k_1}, I_{k_2}) \quad (3)$$

for certain (k_1, k_2) satisfying $1 \leq k_1 < k_2 \leq h$. If taken $\{\hat{\mathbf{U}}_{k_n}\}_{n=3}^h$ as Discrete Fourier Matrices, $\text{rank}_{[k_1, k_2]}(\mathcal{M})$ is referred as to tensor tubal rank of \mathcal{M} [5].

2.2 The Proposed Tensor Completion with A Learnable Tensor Rank Function

From the definition of $\text{rank}_{[k_1, k_2]}(\mathcal{M})$, we can see that it aims to examine the slice-wise tensor rank along the (k_1, k_2) -th mode of transformed data \mathcal{Z} . It allows (1) to investigate the low-rankness of different features in tensor data corresponding to different frequencies separately and jointly.

However, when \mathcal{M} exhibits harsh changes caused by disordered tensor slices, all information in \mathcal{M} tends to collapse into the high-frequency slices in \mathcal{Z} . To handle such situation, we introduce a learnable permutation matrix $\mathbf{P} \in \mathbb{R}^{k_n \times k_n}$ to (2):

$$\mathcal{M} \times_{k_n} \mathbf{P} = \mathcal{Z} \times_{k_3} \hat{\mathbf{U}}_{k_3}^T \cdots \times_{k_n} (\hat{\mathbf{U}}_{k_n} \mathbf{P})^T \times_{k_{n+1}} \cdots \times_{k_h} \hat{\mathbf{U}}_{k_h}^T,$$

and therefore we can get the following model:

$$\begin{aligned} \min_{\mathcal{X}, \mathbf{P}_{k_n}} \quad & \text{rank}_{[k_1, k_2]}(\mathcal{X} \times_{k_n} \mathbf{P}_{k_n}) \\ \text{s.t.} \quad & \Psi_{\mathbb{I}}(\mathcal{M}) = \Psi_{\mathbb{I}}(\mathcal{X}), \quad \mathbf{P}_{k_n}^T \mathbf{P}_{k_n} = \mathbf{I}, \\ & \sum_{i=1}^{k_n} [\mathbf{P}_{k_n}]_{i,j} = 1, \quad \sum_{j=1}^{k_n} [\mathbf{P}_{k_n}]_{i,j} = 1 \text{ for } [\mathbf{P}_{k_n}]_{i,j} \in \{0, 1\}. \end{aligned} \quad (4)$$

This incorporation is aimed at addressing the slice permutation property in tensor completion methods, thus facilitating a more effective exploration of the low-rank property in \mathcal{M} .

Unfortunately, solving (4) is challenging due to the constraints of $\sum_{i=1}^{k_n} [\mathbf{P}_{k_n}]_{i,j} = 1$ and $\sum_{j=1}^{k_n} [\mathbf{P}_{k_n}]_{i,j} = 1$ for $[\mathbf{P}_{k_n}]_{i,j} \in \{0, 1\}$. Therefore, we opt to use a set of learnable unitary matrices $\{\mathbf{U}_{k_n}\}_{n=s+1}^h$ instead, proposing the following tensor completion model:

$$\begin{aligned} \min_{\mathcal{X}, \mathbf{U}_{k_n} (n=s+1, \dots, h)} \quad & \text{rank}_{[k_1, k_2]}(\mathcal{X} \times_{k_{s+1}} \mathbf{U}_{k_{s+1}} \cdots \times_{k_h} \mathbf{U}_{k_h}) \\ \text{s.t.} \quad & \Psi_{\mathbb{I}}(\mathcal{M}) = \Psi_{\mathbb{I}}(\mathcal{X}), \quad \mathbf{U}_{k_n}^T \mathbf{U}_{k_n} = \mathbf{I} (n = s+1, \dots, h), \end{aligned} \quad (5)$$

where \mathcal{X} is a low-rank estimation of the true tensor data \mathcal{M} . Besides simplifying the optimization process of (4), the introduction of unitary matrices enables the model to extract features more effectively for a better study of the low-rankness in tensor data. Therefore, the proposed model can also better handle other scenarios where the initially provided transforms $\{\hat{\mathbf{U}}_{k_n}\}_{n=s+1}^h$ are inadequate, such as videos with irregularly changing content and image sequences with different scenes. Hence, we introduce our learnable tensor rank as

$$\text{rank}_{[k_1, k_2], \tilde{\mathcal{U}}}(\mathcal{X}) = \text{rank}_{[k_1, k_2]}(\tilde{\mathcal{U}}(\mathcal{X})),$$

where $\tilde{\mathcal{U}}(\mathcal{X}) = \mathcal{X} \times_{k_{s+1}} \mathbf{U}_{k_{s+1}} \cdots \times_{k_h} \mathbf{U}_{k_h}$.

2.3 Approximation to The Proposed Tensor Completion by Using A Learnable Tensor Nuclear Norm (TC-SL)

Since the function $\text{rank}_{[1, 2], \tilde{\mathcal{U}}}(\cdot)$ is discrete, it often leads to the NP-hard problem. From the result given in [4], we know that, when $h = 3$ and $\hat{\mathbf{U}}_3$ is orthogonal, $\|\cdot\|_*^{[1, 2]}$ is the tightest convex envelope of $\text{rank}_{[1, 2]}(\cdot)$ on the set $\{\mathcal{A} \mid \|\mathcal{A}\|_2^{[1, 2]} \leq 1\}$, where the definitions of $\|\cdot\|_2^{[k_1, k_2]}$ and $\|\cdot\|_*^{[k_1, k_2]}$ are given in Definition 1. This conclusion can be easily extended to our case, and thus we obtain the Property 1.

Definition 1. For an h -order tensor $\mathcal{A} \in \mathbb{R}^{I_1 \times I_2 \times \cdots \times I_h}$, $\|\mathcal{A}\|_*^{[k_1, k_2]}$ and $\|\mathcal{A}\|_2^{[k_1, k_2]}$ are defined as

$$\|\mathcal{A}\|_*^{[k_1, k_2]} = \sum_{i_{k_3}, i_{k_4}, \dots, i_{k_h}} \|[\mathcal{A}^{T_{k_1, \dots, k_h} \times_{k_3} \hat{\mathbf{U}}_{k_3} \cdots \times_{k_h} \hat{\mathbf{U}}_{k_h}}]_{:, :, i_{k_3}, \dots, i_{k_h}}\|_*$$

and

$$\|\mathcal{A}\|_2^{[k_1, k_2]} = \max_{i_{k_3}, i_{k_4}, \dots, i_{k_h}} \|[\mathcal{A}^{T_{k_1, \dots, k_h} \times_{k_3} \hat{\mathbf{U}}_{k_3} \cdots \times_{k_h} \hat{\mathbf{U}}_{k_h}}]_{:, :, i_{k_3}, \dots, i_{k_h}}\|_2,$$

respectively.

Property 1. For an h -order tensor $\mathcal{A} \in \mathbb{R}^{I_1 \times I_2 \times \cdots \times I_h}$, let us define $\|\mathcal{A}\|_{*, \tilde{\mathcal{U}}}^{[k_1, k_2]}$ and $\|\mathcal{A}\|_{2, \tilde{\mathcal{U}}}^{[k_1, k_2]}$ are defined as $\|\mathcal{A}\|_{*, \tilde{\mathcal{U}}}^{[k_1, k_2]} = \|\tilde{\mathcal{U}}(\mathcal{A})\|_{*, \tilde{\mathcal{U}}}^{[k_1, k_2]}$ and $\|\mathcal{A}\|_{2, \tilde{\mathcal{U}}}^{[k_1, k_2]} = \|\tilde{\mathcal{U}}(\mathcal{A})\|_{2, \tilde{\mathcal{U}}}^{[k_1, k_2]}$, respectively. $\|\cdot\|_{*, \tilde{\mathcal{U}}}^{[k_1, k_2]}$ is the dual norm of tensor $\|\cdot\|_{2, \tilde{\mathcal{U}}}^{[k_1, k_2]}$ norm, and $\|\cdot\|_{*, \tilde{\mathcal{U}}}^{[k_1, k_2]}$ is the tightest convex envelope of $\text{rank}_{[k_1, k_2], \tilde{\mathcal{U}}}(\cdot)$ on the set $\{\mathcal{A} \mid \|\mathcal{A}\|_{2, \tilde{\mathcal{U}}}^{[k_1, k_2]} \leq 1\}$.

Therefore, we derive an approximation to the proposed model (6) by utilizing a learnable tensor nuclear norm based on the prior assumption of slice-wise low-rankness in the transformed data (TC-SL):

$$\min_{\mathcal{X}, \tilde{\mathcal{U}}} \|\mathcal{X}\|_{*, \tilde{\mathcal{U}}}^{[k_1, k_2]} \quad s.t. \quad \Psi_{\mathbb{I}}(\mathcal{M}) = \Psi_{\mathbb{I}}(\mathcal{X}). \quad (6)$$

The theoretical results given in the next subsection will demonstrate the exactly recovery property of TC-SL.

2.4 Theoretical Results

For convenience, we use $\mathcal{U}(\mathcal{A})$ to represent $\mathcal{U}(\mathcal{A}) = \tilde{\mathcal{U}}(\mathcal{A}) \times_{k_3} \hat{\mathcal{U}}_{k_3} \cdots \times_{k_s} \hat{\mathcal{U}}_{k_s}$ for any $\mathcal{A} \in \mathbb{R}^{I_1 \times I_2 \times \cdots \times I_h}$, and we can give the definitions of tensor product and tensor transpose based on \mathcal{U} .

Definition 2. (tensor product for given (k_1, k_2) and \mathcal{U}) For an h -order tensor $\mathcal{A}^{T_{k_1, \dots, k_h}} \in \mathbb{R}^{I_{k_1} \times L \times \cdots \times I_{k_h}}$ and $\mathcal{B}^{T_{k_1, \dots, k_h}} \in \mathbb{R}^{L \times I_{k_2} \times \cdots \times I_{k_h}}$, the tensor product of \mathcal{A} and \mathcal{B} is defined as $\mathcal{A} *_{(k_1, k_2)} \mathcal{B} = \mathcal{U}^{-1}(\mathcal{U}(\mathcal{A}^{T_{k_1, \dots, k_h}}) \odot_f \mathcal{U}(\mathcal{B}^{T_{k_1, \dots, k_h}}))$, where $[\mathcal{U}(\mathcal{A}^{T_{k_1, \dots, k_h}}) \odot_f \mathcal{U}(\mathcal{B}^{T_{k_1, \dots, k_h}})]_{:, :, i_{k_3}, i_{k_4}, \dots, i_{k_h}} = [\mathcal{U}(\mathcal{A}^{T_{k_1, \dots, k_h}})]_{:, :, i_{k_3}, i_{k_4}, \dots, i_{k_h}} [\mathcal{U}(\mathcal{B}^{T_{k_1, \dots, k_h}})]_{:, :, i_{k_3}, i_{k_4}, \dots, i_{k_h}}$.

Definition 3. (tensor transpose for given (k_1, k_2) and \mathcal{U}) For an h -order tensor $\mathcal{A} \in \mathbb{R}^{I_1 \times I_2 \times \cdots \times I_h}$, $\mathcal{A}^{T(k_1, k_2)} \in \mathbb{R}^{I_1 \times \cdots \times I_{k_1-1} \times I_{k_2} \times I_{k_1+1} \times \cdots \times I_{k_2-1} \times I_{k_1} \times I_{k_2+1} \times \cdots \times I_h}$ is tensor transpose of \mathcal{A} along the (k_1, k_2) -th mode such that

$$\begin{aligned} & [\mathcal{U}(\mathcal{A})]_{i_1, \dots, i_{k_1-1}, :, i_{k_1+1}, \dots, i_{k_2-1}, :, i_{k_2+1}, \dots, i_h}^T \\ &= [\mathcal{A}^{T(k_1, k_2)}]_{i_1, \dots, i_{k_1-1}, :, i_{k_1+1}, \dots, i_{k_2-1}, :, i_{k_2+1}, \dots, i_h}. \end{aligned}$$

After defining the tensor product and transpose, we can now consider the corresponding tensor SVD and conduct further analysis of the proposed model. Suppose $\mathcal{M} = \mathcal{U}_0 *_{(k_1, k_2)} \mathcal{S}_0 *_{(k_1, k_2)} \mathcal{V}_0^{T(k_1, k_2)}$ is the skinny t-SVD of tensor data \mathcal{M} . We define $\mathbb{T} = \{\mathcal{U}_0 *_{(k_1, k_2)} \mathcal{Y}^{T(k_1, k_2)} + \mathcal{W} *_{(k_1, k_2)} \mathcal{V}_0^{T(k_1, k_2)}, \mathcal{Y}^{T_{k_1, \dots, k_h}}, \mathcal{W}^{T_{k_1, \dots, k_h}} \in \mathbb{R}^{I_{k_1} \times r \times I_{k_3} \times \cdots \times I_{k_h}}\}$, $P_{\mathbb{T}}$ is the projections onto \mathbb{T} , and \mathbb{T}^\perp is the orthogonal complement of \mathbb{T} . Let $\hat{\mathcal{U}}$ be the invertible transform operator learned by (6). By utilizing the property of subgradient $\partial \|\cdot\|_{*, \tilde{\mathcal{U}}}^{[k_1, k_2]}$ and the duality between $\|\cdot\|_{2, \tilde{\mathcal{U}}}^{[k_1, k_2]}$ and $\|\cdot\|_{*, \tilde{\mathcal{U}}}^{[k_1, k_2]}$, we can get the following results.

Lemma 1. For tensor $\mathcal{A}^{T_{k_1, \dots, k_h}} \in \mathbb{R}^{I_{k_1} \times I_{k_2} \times \cdots \times I_{k_h}}$ with $\text{rank}_{[k_1, k_2], \tilde{\mathcal{U}}}(\mathcal{A}) = r$, if its skinny t-SVD is $\mathcal{A} = \mathcal{U} *_{(k_1, k_2)} \mathcal{S} *_{(k_1, k_2)} \mathcal{V}^{T(k_1, k_2)}$, then the subgradient of $\|\mathcal{A}\|_{*, \tilde{\mathcal{U}}}^{[k_1, k_2]}$ can be given as $\partial \|\mathcal{A}\|_{*, \tilde{\mathcal{U}}}^{[k_1, k_2]} = \{\mathcal{U} *_{(k_1, k_2)} \mathcal{V}^{T(k_1, k_2)} + \mathcal{W} | \mathcal{U}^{T(k_1, k_2)} *_{(k_1, k_2)} \mathcal{W} = \mathbf{0}, \mathcal{W} *_{(k_1, k_2)} \mathcal{V} = \mathbf{0}, \|\mathcal{W}\|_{2, \tilde{\mathcal{U}}}^{[k_1, k_2]} \leq 1\}$.

Theorem 1. If the dual certificate $\mathcal{G} = \Psi_{\mathbb{I}} P_{\mathbb{T}} (P_{\mathbb{T}} \Psi_{\mathbb{I}} P_{\mathbb{T}})^{-1} (\mathcal{U}_0 *_{(k_1, k_2)} \mathcal{V}_0^T)$ satisfies $\|P_{\mathbb{T}^\perp}(\mathcal{G})\|_{2, \tilde{\mathcal{U}}}^{[k_1, k_2]} \leq C_1 < 1$ and $P_{\mathbb{T}} \Psi_{\mathbb{I}} P_{\mathbb{T}} \succ C_2 p \mathcal{I}$, then $\hat{\mathcal{X}}$ obtained by (6) can exactly recover \mathcal{M} , where p is the sampling rate.

The proofs of the Lemma 1 and Theorem 1 are provided in the supplementary material.

2.5 The Proposed Multi-Objective Tensor Completion to Learn The Cross-Dimensional Low-Rankness

From (6), we observe that the definition of TC-SL depends on the choice of k_1 and k_2 , and it considers different kinds of low-rankness in the tensor data by adjusting (k_1, k_2) . However, considering only one mode may result in the loss of correlation information across the remaining modes. To address this issue, we give the following multi-objective model with learnable tensor nuclear norms for tensor completion (MOTC):

$$\min_{\mathcal{X}, \tilde{\mathcal{U}}_{(k_1, k_2)}} \left[\|\mathcal{X}\|_{*, \tilde{\mathcal{U}}_{(k_1, k_2)}}^{[k_1, k_2]} \right]_{1 \leq k_1 < k_2 \leq h} \quad s.t. \quad \Psi_{\mathbb{I}}(\mathcal{M}) = \Psi_{\mathbb{I}}(\mathcal{X}), \quad (7)$$

where $\tilde{\mathcal{U}}_{(k_1, k_2)}(\mathcal{X}) = \mathcal{X} \times_{k_{s+1}} \mathbf{U}_{k_{s+1}}^{(k_1, k_2)} \cdots \times_{k_h} \mathbf{U}_{k_h}^{(k_1, k_2)}$ and $(\mathbf{U}_{k_n}^{(k_1, k_2)})^T \mathbf{U}_{k_n}^{(k_1, k_2)} = \mathbf{I}$ for $n = 1 + s, \dots, h$ and $1 \leq k_1 < k_2 \leq h$. In MOTC, the multiple objective functions $\|\mathcal{X}\|_{*, \tilde{\mathcal{U}}_{(k_1, k_2)}}^{[k_1, k_2]}$ ($1 \leq k_1 < k_2 \leq h$) are utilized to examine the low-rankness of tensor data from its various dimensions.

3 Optimization Algorithm

In this section, we provide a detailed discussion of the optimization for (6) and (7).

3.1 Alternating Proximal Multiplier Method (APMM) for TC-SL

To solve the problem (6), we introduce auxiliary variables $\mathcal{E} \in \mathbb{E} = \{\mathcal{E} | \Psi_{\mathbb{I}}(\mathcal{E}) = \mathbf{0}\}$ and \mathcal{Z} such that $\mathcal{X} = \mathcal{Z} \times_{k_{s+1}} \mathbf{U}_{k_{s+1}}^T \cdots \times_{k_h} \mathbf{U}_{k_h}^T$. Therefore, we turn to solve the following equivalence problem:

$$\min_{\mathcal{Z}, \mathbf{U}_{k_n}^T \mathbf{U}_{k_n} = \mathbf{I} (n=s+1, \dots, h)} \|\mathcal{Z}\|_*^{[k_1, k_2]} \quad s.t. \quad \Psi_{\mathbb{I}}(\mathcal{M}) = \mathcal{Z} \times_{k_{s+1}} \mathbf{U}_{k_{s+1}}^T \cdots \times_{k_h} \mathbf{U}_{k_h}^T + \mathcal{E}. \quad (8)$$

The Augmented Lagrangian function of (8) is formulated as

$$\begin{aligned} & \mathcal{L}(\mathcal{Z}, \{\mathbf{U}_{k_n}\}_{n=s+1}^h, \mathcal{E}, \mathcal{Y}, \mu) \\ &= \|\mathcal{Z}\|_*^{[k_1, k_2]} + \langle \Psi_{\mathbb{I}}(\mathcal{M}) - \mathcal{Z} \times_{k_{s+1}} \mathbf{U}_{k_{s+1}}^T \cdots \times_{k_h} \mathbf{U}_{k_h}^T - \mathcal{E}, \mathcal{Y} \rangle \\ &+ \frac{\mu}{2} \|\Psi_{\mathbb{I}}(\mathcal{M}) - \mathcal{Z} \times_{k_{s+1}} \mathbf{U}_{k_{s+1}}^T \cdots \times_{k_h} \mathbf{U}_{k_h}^T - \mathcal{E}\|_F^2, \end{aligned} \quad (9)$$

where $\mathcal{E} \in \mathbb{E}$, \mathcal{Y} is Lagrange multiplier, and μ is a positive scalar. We solve (8) iteratively by combining the proximal algorithm with the Alternating Direction Method of Multipliers (APMM) that consists of the following steps:

$$\left\{ \begin{array}{l} \mathcal{Z}^{(t+1)} = \arg \min_{\mathcal{Z}} \mathcal{L}(\mathcal{Z}, \{\mathbf{U}_{k_n}^{(t)}\}_{n=s+1}^h, \mathcal{E}^{(t)}, \mathcal{Y}^{(t)}, \mu^{(t)}) + \frac{\eta^{(t)}}{2} \|\mathcal{Z}^{(t)} - \mathcal{Z}\|_F^2; \\ \mathbf{U}_{k_{n_0}}^{(t+1)} = \arg \min_{\mathbf{U}_{k_{n_0}}^T \mathbf{U}_{k_{n_0}} = \mathbf{I}} \mathcal{L}(\mathcal{Z}^{(t+1)}, \{\mathbf{U}_{k_n}^{(t+1)}\}_{n=s+1}^{n_0-1}, \mathbf{U}_{k_{n_0}}, \{\mathbf{U}_{k_n}^{(t)}\}_{n=n_0+1}^h, \mathcal{E}^{(t)}, \\ \quad \mathcal{Y}^{(t)}, \mu^{(t)}) + \frac{\eta^{(t)}}{2} \|\mathbf{U}_{k_{n_0}}^{(t)} - \mathbf{U}_{k_{n_0}}\|_F^2, \quad (s+1 \leq n_0 \leq h); \\ \mathcal{E}^{(t+1)} = \arg \min_{\mathcal{E} \in \mathbb{E}} \mathcal{L}(\mathcal{Z}^{(t+1)}, \{\mathbf{U}_{k_n}^{(t+1)}\}_{n=s+1}^h, \mathcal{E}, \mathcal{Y}^{(t)}, \mu^{(t)}) + \frac{\eta^{(t)}}{2} \|\mathcal{E} - \mathcal{E}^{(t)}\|_F^2; \\ \mathcal{Y}^{(t+1)} = \mu^{(t)} (\Psi_{\mathbb{I}}(\mathcal{M}) - \mathcal{X}^{(t+1)} - \mathcal{E}^{(t+1)}) + \mathcal{Y}^{(t)}; \\ \mu^{(t+1)} = \min(\bar{\mu}, \rho \mu^{(t)}) \text{ and } \eta^{(t+1)} = \min(\bar{\eta}, \rho \eta^{(t)}). \end{array} \right.$$

We repeat the above steps until convergence is achieved. The entire process is detailed in Algorithm 1².

3.1.1 Computational Complexity

The most time-consuming steps in the algorithm 1 are the computations of \mathcal{Z} , and \mathbf{U}_{k_n} . Since the computational complexity of n-mode product of $\hat{\mathcal{P}} \in \mathbb{R}^{I_1 \times I_2 \times \cdots \times I_h}$ and $\mathbf{U}_n \in \mathbb{R}^{I_n \times I_n}$ is $\mathcal{O}(I_n I_1 I_2 \cdots I_h)$, the complexity of the computation of \mathcal{Z} is $\mathcal{O}(h I_{(1)} I_1 I_2 \cdots I_h)$, where $I_{(1)} = \max_k(I_k)$. Besides, the complexity of the computation of \mathbf{U}_{k_n} is $\mathcal{O}((h-1)I_{(1)} I_1 I_2 \cdots I_h + I_k^2 I_1 I_2 \cdots I_h)$, therefore the overall computational complexity of each iteration of Algorithm 1 is $\mathcal{O}((h-s)(h+I_{(1)}-1)I_{(1)} I_1 I_2 \cdots I_h + h I_{(1)} I_1 I_2 \cdots I_h)$.

3.1.2 Convergence Analysis

Although the optimization problem (8) is non-convex because of the constraints $\mathbf{U}_{k_n}^T \mathbf{U}_{k_n} = \mathbf{I} (n=s+1, s+2, \dots, h)$ and the global optimality for (8) is hardly guaranteed, we can still prove some excellent convergence properties of the Algorithm 1, as stated in the following theorem.

Theorem 2. For the sequence $\{\{\mathcal{Z}^{(t)}, \{\mathbf{U}_{k_n}^{(t)}\}_{n=s+1}^h, \mathcal{E}^{(t)}, \mathcal{Y}^{(t)}, \mu^{(t)}\}\}$ generated by the proposed algorithm 1, we have the following properties if $\{\mathcal{Y}^{(t)}\}$ is bounded, $\sum_{t=1}^{\infty} (\mu^{(t)})^{-2} \mu^{(t+1)} < +\infty$ and $\lim_{n \rightarrow \infty} \mu^{(n)} \sum_{t=n}^{\infty} (\eta^{(t)})^{-1/2} = 0$.

(i) $\lim_{t \rightarrow \infty} \Psi_{\mathbb{I}}(\mathcal{M}) - \mathcal{X}^{(t)} - \mathcal{E}^{(t)} = \mathbf{0}$, where $\mathcal{X}^{(t)} = \mathcal{Z}^{(t)} \times_{k_h} (\mathbf{U}_{k_h}^{(t)})^T \cdots \times_{k_{s+1}} (\mathbf{U}_{k_{s+1}}^{(t)})^T$.

(ii) $\{\{\mathcal{Z}^{(t)}, \{\mathbf{U}_{k_n}^{(t)}\}_{n=s+1}^h, \mathcal{X}^{(t)}, \mathcal{E}^{(t)}\}\}$ is bounded.

(iii) $\sum_{t=1}^{\infty} \eta^{(t)} \|\{\mathcal{Z}^{(t)}, \{\mathbf{U}_{k_n}^{(t)}\}_{n=s+1}^h, \mathcal{E}^{(t)}\} - \{\mathcal{Z}^{(t+1)}, \{\mathbf{U}_{k_n}^{(t+1)}\}_{n=s+1}^h, \mathcal{E}^{(t+1)}\}\|_F^2$ is convergent. Thus, we have

$$\|\{\mathcal{Z}^{(t)}, \{\mathbf{U}_{k_n}^{(t)}\}_{n=s+1}^h, \mathcal{E}^{(t)}\} - \{\mathcal{Z}^{(t+1)}, \{\mathbf{U}_{k_n}^{(t+1)}\}_{n=s+1}^h, \mathcal{E}^{(t+1)}\}\|_F^2 \leq \mathcal{O}\left(\frac{1}{\eta^{(t)}}\right).$$

² $(\mathcal{A}, \tau)_{\times, (k_1, k_2)}$ represent the tensor singular value thresholding operation with parameter τ [2].

Algorithm 1: APMM-based Iterative Solver to (8)

Input: $\Psi_{\mathbb{I}}(\mathcal{M})$, $\{\mathbf{U}_{k_n}^{(0)}\}_{n=s+1}^h$, $\{\hat{\mathbf{U}}_{k_n}^{(0)}\}_{n=1}^s$, $\mathcal{E}^{(0)}$, $\mathcal{Y}^{(0)}$, $t = 0$, $\rho_\mu, \rho_\eta > 1$, $\bar{\mu}, \bar{\eta}$, $\mu^{(0)}$, and $\eta^{(0)}$.

Output: $\mathcal{Z}^{(t+1)}$, $\{\mathbf{U}_{k_n}^{(t+1)}\}_{n=s+1}^h$, and $\mathcal{X}^{(t+1)} = \mathcal{Z}^{(t+1)} \times_{k_h} \mathbf{U}_{k_h}^{(t+1)T} \times_{k_{h-1}} \cdots \times_{k_{s+1}} \mathbf{U}_{k_{s+1}}^{(t+1)T}$.

1. **While not converge do**

2. Calculate $\mathcal{Z}^{(t+1)}$ by $\mathcal{Z}^{(t+1)} = \left(\frac{\mu^{(t)} \hat{\mathcal{P}} \times_{k_{s+1}} \mathbf{U}_{k_{s+1}}^{(t)} \cdots \times_{k_h} \mathbf{U}_{k_h}^{(t)} + \eta^{(t)} \mathcal{Z}^{(t)}}{\mu^{(t)} + \eta^{(t)}}, \frac{1}{\mu^{(t)} + \eta^{(t)}} \right)_{\times, (k_1, k_2)}$;

3. Compute $\mathbf{U}_{k_n}^{(t+1)}$ by $\mathbf{U}_{k_n}^{(t+1)} = \mathbf{U}\mathbf{V}^T$ ($n = s+1, \dots, h$), where \mathbf{U} and \mathbf{V} can be obtained by SVD of $\mu^{(t)} \mathcal{A}_{(k_n)} \mathcal{B}_{(k_n)}^T + \eta^{(t)} \mathbf{U}_{k_n}^{(t)}$: $\mu^{(t)} \mathcal{A}_{(k_n)} \mathcal{B}_{(k_n)}^T + \eta^{(t)} \mathbf{U}_{k_n}^{(t)} = \mathbf{U}\Sigma\mathbf{V}^T$, $\mathcal{A} = \mathcal{Z}^{(t+1)} \times_{k_h} \mathbf{U}_{k_h}^{(t)T} \cdots \times_{k_{n+1}} \mathbf{U}_{k_{n+1}}^{(t)T}$, and $\mathcal{B} = \hat{\mathcal{P}} \times_{s+1} \mathbf{U}_{k_{s+1}}^{(t+1)} \cdots \times_{k_{n-1}} \mathbf{U}_{k_{n-1}}^{(t+1)}$;

4. Calculate $\mathcal{X}^{(t+1)}$ by $\mathcal{X}^{(t+1)} = \mathcal{Z}^{(t+1)} \times_{k_h} \mathbf{U}_{k_h}^{(t+1)T} \times_{k_{h-1}} \cdots \times_{k_{s+1}} \mathbf{U}_{k_{s+1}}^{(t+1)T}$;

5. Calculate $\mathcal{E}^{(t+1)}$ by

$$\mathcal{E}^{(t+1)} = \Psi_{\mathbb{I}^c} \left(\frac{1}{\mu^{(t)} + \eta^{(t)}} (\mu^{(t)} (\Psi_{\mathbb{I}}(\mathcal{M}) - \mathcal{X}^{(t+1)} + \frac{1}{\mu^{(t)}} \mathcal{Y}^{(t)}) + \eta^{(t)} \mathcal{E}^{(t)}) \right);$$

6. Calculate $\mathcal{Y}^{(t+1)}$ by $\mathcal{Y}^{(t+1)} = \mu^{(t)} (\Psi_{\mathbb{I}}(\mathcal{M}) - \mathcal{X}^{(t+1)} - \mathcal{E}^{(t+1)}) + \mathcal{Y}^{(t)}$;

7. Compute $\mu^{(t+1)}$ and $\eta^{(t+1)}$ by $\mu^{(t+1)} = \min(\bar{\mu}, \rho_\mu \mu^{(t)})$ and $\eta^{(t+1)} = \min(\bar{\eta}, \rho_\eta \eta^{(t)})$, respectively;

8. Check the convergence condition: $\|\mathcal{Z}^{(t+1)} - \mathcal{Z}^{(t)}\|_\infty < \varepsilon$, $\|\mathcal{X}^{(t+1)} - \mathcal{X}^{(t)}\|_\infty < \varepsilon$,

$\|\mathbf{U}_{k_n}^{(t+1)} - \mathbf{U}_{k_n}^{(t)}\|_\infty < \varepsilon$ for $n = s+1, s+2, \dots, h$;

9. $t = t+1$.

10. **end while**

(iv) $\lim_{t \rightarrow \infty} \|\mathcal{Y}^{(t+1)} - \mathcal{Y}^{(t)}\|_F = 0$.

(v) Let $[\mathcal{Z}^*, \{\mathbf{U}_{k_n}^*\}_{n=s+1}^h, \mathcal{E}^*, \mathcal{Y}^*]$ be any limit point of $\{[\mathcal{Z}^{(t)}, \{\mathbf{U}_{k_n}^{(t)}\}_{n=s+1}^h, \mathcal{E}^{(t)}, \mathcal{Y}^{(t)}]\}$. Then, $[\mathcal{Z}^*, \{\mathbf{U}_{k_n}^*\}_{n=s+1}^h, \mathcal{E}^*, \mathcal{Y}^*]$ is a KKT point to (8).

Please refer to the supplementary material of this paper for the proof of the Theorem 2. Theorem 2 shows that, if $\{\mathcal{Y}^{(t)}\}$ is bounded, the sequence $[\mathcal{Z}^{(t)}, \{\mathbf{U}_{k_n}^{(t)}\}_{n=s+1}^h, \mathcal{E}^{(t)}]$ generated by the proposed algorithm 1 is Cauchy convergent, with a convergence rate of at least $\mathcal{O}(\frac{1}{\eta^{(t)}})$. Moreover, any accumulation point of the sequence converges to the KKT point of (8).

3.2 APMM-based Heuristic Method for Solving MOTC

To solve MOTC, we iteratively update $\mathbf{U}_{k_n}^{(k_1, k_2)}$ ($n = 1 + s, \dots, h$, $1 \leq k_1 < k_2 \leq h$) and \mathcal{X} in (7) by solving the following optimization problems:

$$\hat{\mathcal{U}}_{(k_1, k_2)} = \arg \min_{\tilde{\mathcal{U}}_{(k_1, k_2)}} \|\hat{\mathcal{X}}\|_{*, \tilde{\mathcal{U}}_{(k_1, k_2)}}^{[k_1, k_2]} \quad (10)$$

and

$$\hat{\mathcal{X}} = \arg \min_{\mathcal{X}} \left[\|\mathcal{X}\|_{*, \hat{\mathcal{U}}_{(k_1, k_2)}}^{(k_1, k_2)} \right]_{1 \leq k_1 < k_2 \leq h} \text{ s.t. } \Psi_{\mathbb{I}}(\mathcal{M}) = \Psi_{\mathbb{I}}(\mathcal{X}), \quad (11)$$

respectively. We use the proposed APMM for solving (10), and the non-dominated sorting genetic algorithm (NSGA-II) [?] presented in Algorithm 2 for solving (11). These two steps are used for the learning of the tensor nuclear norm functions and the low rank estimation, respectively. It is worth noting that both updating the $\hat{\mathcal{U}}_{(k_1, k_2)}$ for each (k_1, k_2) and evaluating the individuals in Algorithm 2 can be proceed in parallel, which can accelerate the whole optimization for MOTC.

Algorithm 2: NSGA-II-based framework for solving (11)

Input: $\Psi_{\mathbb{I}}(\mathcal{M})$, $\{\hat{\mathcal{U}}_{(k_1, k_2)}\}_{1 \leq k_1 < k_2 \leq h}$, IterMax, and $t = 0$.**Output:** $\hat{\mathcal{X}}$

1. **Initialize:** population $\mathbb{P}^{(0)}$
 2. Evaluate $\left[\|\mathcal{X}\|_{*}^{[k_1, k_2]} \right]_{1 \leq k_1 < k_2 \leq h}$ for each $\mathcal{X} \in \mathbb{P}^{(t)}$;
 3. Sorting individuals by their non-domination ranks and crowding distance, and obtaining the first front \mathbb{F}_1 ;
 4. Selecting parents and applying crossover and mutation to create offspring;
 5. Obtaining the next generation by truncating the sorted individuals (including offspring population) and update the first front \mathbb{F}_1 ;
 6. $t = t + 1$;
 7. Repeat steps 2-6 until $t = \text{IterMax}$;
 8. $\hat{\mathcal{X}} =$ average sum of the individuals that belong to \mathbb{F}_1 .
-

Table 2: Comparing the PSNR results by different methods on *BSD* at different sampling rates p .

| Sampling Rate p | TNN-DCT | TNN-DFT | SNN | KBR | WSTNN | HTNN-DCT | TC-SL | MOTC |
|-------------------|---------|---------|-------|-------|-------|----------|-------|--------------|
| 0.3 | 23.25 | 23.21 | 21.86 | 25.45 | 25.75 | 25.21 | 26.32 | 27.53 |
| 0.5 | 27.25 | 27.20 | 25.50 | 31.57 | 31.07 | 30.72 | 31.55 | 33.25 |
| 0.7 | 32.04 | 31.95 | 29.84 | 38.81 | 37.11 | 38.22 | 38.33 | 39.97 |
| Average | 27.51 | 27.45 | 25.73 | 31.94 | 31.31 | 31.38 | 32.06 | 33.58 |

4 Experimental Results

In this section, we compared the TC-SL and MOTC with several state-of-the-art methods, including TNN-DCT [4], TNN-DFT [5], SNN [18], KBR [26], WSTNN [19], and HTNN-DCT [20], in the context of color video inpainting and images inpainting. Below are brief explanations for all eight methods:

- **TNN-DCT and TNN-DFT** are three-order tensor completion methods;
- **HTNN-DCT and TC-SL** are higher-order tensor completion methods, but they consider low-rankness along only one dimension of the tensor;
- **SNN, KBR, WSTNN, and MOTC** are higher-order tensor completion methods that have considered low-rankness across various dimensions of the tensor. SNN and KBR are Tucker decomposition-based methods.

For the three-order tensor methods, the data tensors were constructed by the mode-(1,2) unfolding tensor, *i.e.*, $[\Psi_{\mathbb{I}}(\mathcal{M})]_{(1,2)} \in \mathbb{R}^{I_1 \times I_2 \times I_3 I_4}$. Here, $I_1 \times I_2$ represents the size of each image (frame), $I_3 = 3$ is RGB channel number of each image, and I_4 is the number of images (frames). For a fair comparison, we implemented the compared methods using the code provided by the respective authors in our experimental environment. **The code for our proposed method is submitted as supplementary material.**

We used the Peak Signal-To-Noise Ratio (PSNR) to evaluate the performance of different methods in tensor completion. To ensure the reliability of our experiments, we conducted each experiment five times and reported the average results as the final outcomes. The best results for each case are shown in bold. All experiments were implemented using Matlab R2022b.

4.1 Images Inpainting

4.1.1 Image Sequences With Various Scenes

In this subsection, we evaluated different tensor completion methods on *Berkeley Segmentation Dataset (BSD)*³ [27], which includes color images with different scenes. Following the experiment setting in [2], we randomly selected 50 color images for testing.

Table 2 presents the PSNR values achieved by each method. From the table, most of the higher tensor methods (KBR, WSTNN, HTNN-DCT, TC-SL, and MOTC) consistently outperform the three-order tensor methods (TNN-DCT and

³<https://www2.eecs.berkeley.edu/Research/Projects/CS/vision/bsds/>

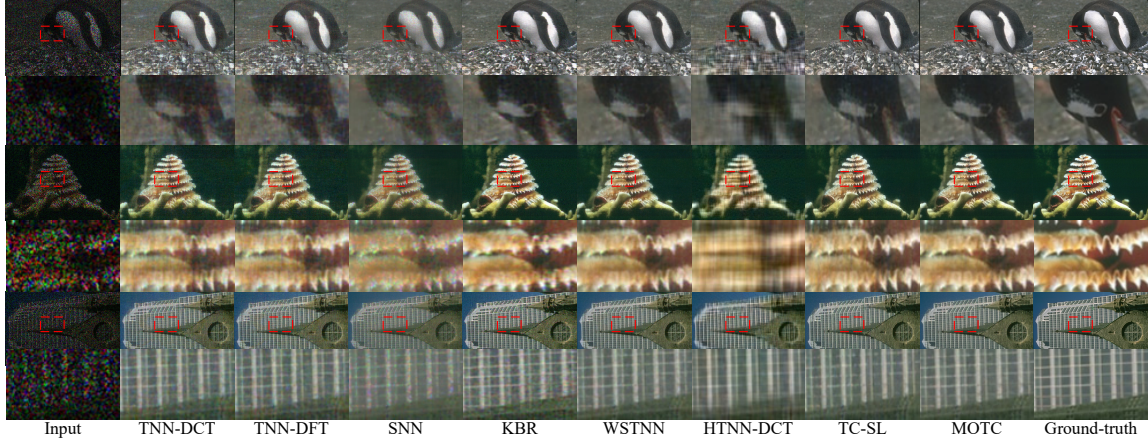


Figure 2: Examples of images inpainting by different methods on the BSD dataset with sampling rate $p = 0.3$. **Best viewed in $\times 2$ sized color pdf file.**

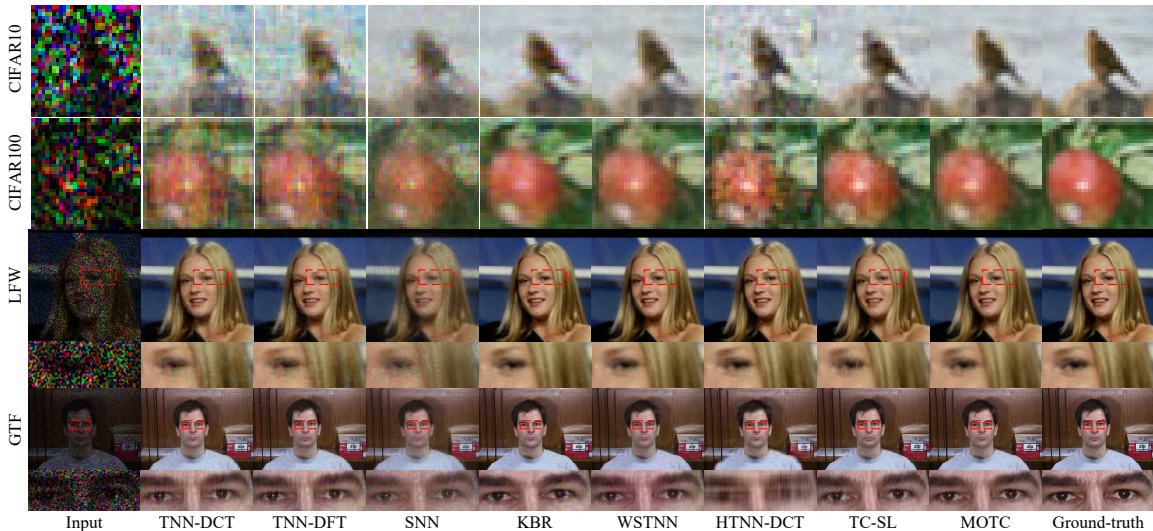


Figure 3: Examples of images inpainting by different methods on three dataset with sampling rate $p = 0.3$. **Best viewed in $\times 2$ sized color pdf file.**

TNN-DFT) across all cases. It indicates that high-order tensor methods are more effective in accurately capturing the low-rank structure in four-order tensor data. Additionally, both TC-SL and MOTC, the proposed methods, exhibit the best performance across all cases, surpassing other methods by approximately 1.5 dB for $p \in \{0.3, 0.5\}$. Visual examples of images inpainting by different methods at a sampling rate $p = 0.3$ are presented in Fig. 2. As observed in the figure, the visual results obtained from WSTNN, TC-SL, and MOTC demonstrate superior reconstruction quality and preservation of finer details compared to other methods.

4.1.2 Image Sequences With Random Shuffling

In this subsection, we evaluated different tensor completion methods using four image classification datasets: *CIFAR10*⁴ [?], *CIFAR100* [?], *Labeled Faces in the Wild (LFW)*⁵, and *Georgia Tech Face database (GTF)*⁶. Due to constraints in computing resources, we utilized subsets of the datasets. Specifically, for CIFAR10 and CIFAR100, we sampled the first 50 images and 5 images for each category, respectively, resulting in two subsets of 500 images. For

⁴<https://www.cs.toronto.edu/~kriz/cifar.html>

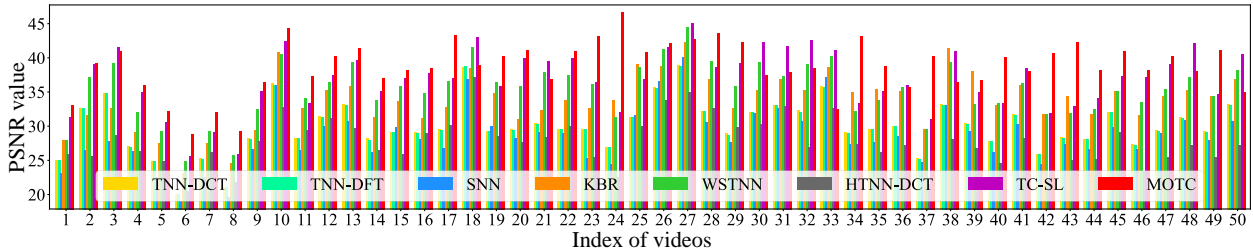
⁵<http://vis-www.cs.umass.edu/lfw/>

⁶http://www.anefian.com/research/face_reco.htm

Table 3: Comparing the PSNR results by different methods at sampling rates $p = 0.3$.

| Data | TNN-DCT | TNN-DFT | SNN | KBR | WSTNN | HTNN-DCT | TC-SL | MOTC |
|----------|---------|---------|-------|-------|-------|----------|-------|--------------|
| CIFAR10 | 19.59 | 19.54 | 20.71 | 24.08 | 25.02 | 22.12 | 24.63 | 26.46 |
| CIFAR100 | 19.39 | 19.31 | 20.70 | 24.15 | 24.76 | 21.71 | 24.50 | 26.16 |
| LFW | 27.49 | 27.45 | 22.48 | 33.47 | 34.33 | 30.15 | 31.57 | 35.67 |
| GTF | 25.46 | 25.41 | 23.54 | 25.83 | 26.66 | 22.11 | 32.10 | 33.56 |
| Average | 22.98 | 22.92 | 21.85 | 26.88 | 27.69 | 24.02 | 28.20 | 30.46 |

Figure 4: Comparing PSNR by different methods on the 50 video segments at a sampling rate $p = 0.3$.



LFW, we selected the first 50 classes, and for GTF, we selected the first five classes. Random shuffling was applied to the image sequences before testing. All PSNR results are provided in Table 3.

From the results, both proposed methods (TC-SL and MOTC) achieved the best performance on average. Upon comparing HTNN-DCT and TC-SL, it is observed that the average performance of the proposed TC-SL surpasses HTNN-DCT by more than 4 dB. It indicates that our method, incorporating a learnable tensor norm, effectively handles SPV in t-SVD-based methods. Among all methods, MOTC achieves the best performance across all cases. Particularly noteworthy is the average PSNR result obtained by MOTC, outperforming other methods by more than 2.5 dB on average. Additionally, as observed in Fig. 3, the visual results obtained from MOTC exhibit smoother transitions and better restoration of intricate textures. All results highlights the effectiveness of the proposed framework.

4.1.3 Results Analysis

These results suggest that the proposed MOTC is able to exploit the correlations of tensor data along different dimensions effectively and can more accurately exploit the low-rank structure of four-order tensor data (the one with non-continue change) than other methods. The superiority of TC-SL and MOTC over other methods can be attributed to the introduction of both the given transforms from smooth priors and learnable unitary matrices, which enable it to better handle the non-smooth in tensor data caused by random shuffling image sequences (such as *CIFAR10*, *CIFAR100*, *LFW*, and *GTF*) or the concatenation of different scene images (such as *BSD*) and capture the underlying low-rank structures in the tensor data more effectively.

4.2 Color Video Inpainting for Video with Rapidly Changing Frames

We evaluated all tensor completion methods on the randomly selected 50 color video segments with the rapidly changing frames from the ‘run’ category of the *HMDB51*⁷.

We presented the PSNR values of all methods on the 50 video segments in Fig. 4 and report their average results in Table 4. The results show a significant improvement achieved by our methods (TC-SL and MOTC) for color video inpainting. For some videos (such as the 24-th, 34-th, 42-th, 43-th), as shown in the Fig. 4, MOTC even achieved a 5-10 dB improvement in PSNR value! Furthermore, the average results obtained by MOTC outperform the third-best method by more than 3.5 dB on average, where the second-best method is TC-SL. The comparison between TC-SL and MOTC

⁷<https://serre-lab.clps.brown.edu/resource/hmdb-a-large-human-motion-database/>

Table 4: Comparing the average PSNR by different methods on the 50 video segments at a sampling rate $p = 0.3$.

| Video | TNN-DCT | TNN-DFT | SNN | KBR | WSTNN | HTNN-DCT | TC-SL | MOTC |
|---------|---------|---------|-------|-------|-------|----------|-------|--------------|
| Average | 30.01 | 29.91 | 28.59 | 33.76 | 35.28 | 27.71 | 36.82 | 38.74 |



Figure 5: Examples of video inpainting by different methods on *HMDB51* dataset for case of $p = 0.3$. **Best viewed in $\times 2$ sized color pdf file.**

demonstrates the effectiveness of the proposed multi-objective tensor recovery framework in exploring the low-rankness of high-order tensor data across its various dimensions. Additionally, comparing tensor methods that consider the low-rankness of a tensor along with only one of its dimensions, TC-SL has achieved a 6.5 dB improvement! This substantial improvement showcased by TC-SL in color video inpainting provides strong evidence for its effectiveness in high-order tensor completion, particularly in scenarios involving non-smooth changes between tensor slices. Visual examples of video inpainting by different methods are presented in Fig. 5. As we can see from the Fig. 5, even for cases that are hardly recognized by humans, MOTC can still reconstruct the video well and restore more detailed information than other tensor completion methods.

5 Conclusions

In this work, we propose a multi-objective tensor recovery framework with a learnable tensor nuclear norm, which is solved by the proposed APM-based heuristic optimization. This framework first provides an effective solution for addressing the non-smooth challenge in t-SVD-based methods. Thanks to our proposed methods, there has no longer a need to introduce $\binom{h}{2}$ variables and tune weighted parameters to analyze the correlation information of tensors across different dimensions. Experimental results in real-world applications demonstrate the superiority of our methods over previous methods, especially for the tensor data with non-smooth changes.

It is worth noting that the proposed tensor completion methods and framework extend beyond tensor completion alone and are applicable to various tensor analysis problems and tasks, including data processing, representation learning, sketching, and clustering. Many directions for future work are possible.

References

- [1] Ibrahim Kajo, Nidal Kamel, and Yassine Ruichek. Self-motion-assisted tensor completion method for background initialization in complex video sequences. *IEEE Transactions on Image Processing*, 29:1915–1928, 2019.
- [2] Canyi Lu, Jiashi Feng, Yudong Chen, Wei Liu, Zhouchen Lin, and Shuicheng Yan. Tensor robust principal component analysis with a new tensor nuclear norm. *IEEE Transactions on Pattern Analysis and Machine Intelligence*, 42(4):925–938, 2019.
- [3] Zemin Zhang, Gregory Ely, Shuchin Aeron, Ning Hao, and Misha Kilmer. Novel methods for multilinear data completion and de-noising based on tensor-svd. In *Proceedings of the IEEE Conference on Computer Vision and Pattern Recognition*, pages 3842–3849, 2014.
- [4] Canyi Lu, Xi Peng, and Yunchao Wei. Low-rank tensor completion with a new tensor nuclear norm induced by invertible linear transforms. In *Proceedings of the IEEE/CVF Conference on Computer Vision and Pattern Recognition*, pages 5996–6004, 2019.
- [5] Canyi Lu, Jiashi Feng, Zhouchen Lin, and Shuicheng Yan. Exact low tubal rank tensor recovery from gaussian measurements. *arXiv preprint arXiv:1806.02511*, 2018.

- [6] Baburaj Madathil and Sudhish N George. Twist tensor total variation regularized-reweighted nuclear norm based tensor completion for video missing area recovery. *Information Sciences*, 423:376–397, 2018.
- [7] Emmanuel J Candes and Yaniv Plan. Matrix completion with noise. *Proceedings of the IEEE*, 98(6):925–936, 2010.
- [8] Emmanuel J Candès and Benjamin Recht. Exact matrix completion via convex optimization. *Foundations of Computational Mathematics*, 9(6):717–772, 2009.
- [9] Emmanuel J Candès, Xiaodong Li, Yi Ma, and John Wright. Robust principal component analysis? *Journal of the ACM (JACM)*, 58(3):1–37, 2011.
- [10] Venkat Chandrasekaran, Sujay Sanghavi, Pablo A Parrilo, and Alan S Willsky. Sparse and low-rank matrix decompositions. *IFAC Proceedings Volumes*, 42(10):1493–1498, 2009.
- [11] Huan Xu, Constantine Caramanis, and Sujay Sanghavi. Robust pca via outlier pursuit. *IEEE Transactions on Information Theory*, 58(5):3047–3064, 2012.
- [12] John Wright, Arvind Ganesh, Shankar R Rao, Yigang Peng, and Yi Ma. Robust principal component analysis: Exact recovery of corrupted low-rank matrices via convex optimization. In *Neural Information Processing Systems*, volume 58, pages 289–298, 2009.
- [13] Frank L Hitchcock. The expression of a tensor or a polyadic as a sum of products. *Journal of Mathematics and Physics*, 6(1-4):164–189, 1927.
- [14] Frank L Hitchcock. Multiple invariants and generalized rank of a p-way matrix or tensor. *Journal of Mathematics and Physics*, 7(1-4):39–79, 1928.
- [15] Tamara G Kolda and Brett W Bader. Tensor decompositions and applications. *SIAM Review*, 51(3):455–500, 2009.
- [16] Ledyard R Tucker. Implications of factor analysis of three-way matrices for measurement of change. *Problems in measuring change*, 15(122-137):3, 1963.
- [17] Silvia Gandy, Benjamin Recht, and Isao Yamada. Tensor completion and low-n-rank tensor recovery via convex optimization. *Inverse Problems*, 27(2):025010, 2011.
- [18] Ji Liu, Przemyslaw Musialski, Peter Wonka, and Jieping Ye. Tensor completion for estimating missing values in visual data. *IEEE Transactions on Pattern Analysis Machine Intelligence*, 35(1):208–220, 2013.
- [19] Yu-Bang Zheng, Ting-Zhu Huang, Xi-Le Zhao, Tai-Xiang Jiang, Teng-Yu Ji, and Tian-Hui Ma. Tensor n-tubal rank and its convex relaxation for low-rank tensor recovery. *Information Sciences*, 532:170–189, 2020.
- [20] Wenjin Qin, Hailin Wang, Feng Zhang, Jianjun Wang, Xin Luo, and Tingwen Huang. Low-rank high-order tensor completion with applications in visual data. *IEEE Transactions on Image Processing*, 31:2433–2448, 2022.
- [21] Ibrahim Kajo, Nidal Kamel, Yassine Ruichek, and Aamir Saeed Malik. Svd-based tensor-completion technique for background initialization. *IEEE Transactions on Image Processing*, 27(6):3114–3126, 2018.
- [22] Jingjing Zheng, Xiaoqin Zhang, Wenzhe Wang, and Xianta Jiang. Handling slice permutations variability in tensor recovery. *Proceedings of the AAAI Conference on Artificial Intelligence*, 36(3):3499–3507, 2022.
- [23] Hao Kong, Canyi Lu, and Zhouchen Lin. Tensor q-rank: new data dependent definition of tensor rank. *Machine Learning*, 110(7):1867–1900, 2021.
- [24] John Wright, Allen Y Yang, Arvind Ganesh, S Shankar Sastry, and Yi Ma. Robust face recognition via sparse representation. *IEEE transactions on pattern analysis and machine intelligence*, 31(2):210–227, 2008.
- [25] Hui Zou, Trevor Hastie, and Robert Tibshirani. Sparse principal component analysis. *Journal of computational and graphical statistics*, 15(2):265–286, 2006.
- [26] Qi Xie, Qian Zhao, Deyu Meng, and Zongben Xu. Kronecker-basis-representation based tensor sparsity and its applications to tensor recovery. *IEEE transactions on pattern analysis and machine intelligence*, 40(8):1888–1902, 2017.
- [27] David Martin, Charless Fowlkes, Doron Tal, and Jitendra Malik. A database of human segmented natural images and its application to evaluating segmentation algorithms and measuring ecological statistics. In *Proceedings Eighth IEEE International Conference on Computer Vision.*, volume 2, pages 416–423, 2001.